EXPERIMENTAL IDENTIFICATION OF A NONLINEAR SPACE STRUCTURE

J.P. Noel[*], L. Renson[*], G. Kerschen[*], and A. Newerla[**]

[*] *Space Structures and Systems Laboratory (S3L), Department of Aerospace and Mechanical Engineering*
University of Liège, Liège, Belgium
[**] *Structures Section, European Space Agency (ESTEC), Noordwijk, The Netherlands*

ABSTRACT

The present paper addresses the experimental identification of a nonlinear space structure, the SmallSat spacecraft developed by EADS-Astrium. The nonlinear component comprises an inertia wheel mounted on a support, the motion of which is constrained by eight elastomer plots and mechanical stops. Robust techniques are applied to measured data to detect, characterise and quantify nonlinear behaviour.

Key words: Nonlinear system identification, space structure, experimental data.

1. INTRODUCTION

Many nonlinear system identification methods have been introduced in the technical literature during the last thirty years. Among the well-established approaches, there exist the restoring force surface method [1] in the time domain, the conditioned reverse path method [2] in the frequency domain or the wavelet transform [3] as a time-frequency analysis tool. However, few of these methods were applied to real-life structures. In this context, the objective of the present paper is to address the experimental identification of a large-scale space structure, the SmallSat spacecraft developed by EADS-Astrium. A careful progression through the different steps of system identification in nonlinear structural dynamics [4], namely detection, characterisation and parameter estimation, is carried out. Once nonlinear behaviour is detected, a nonlinear system is said to be characterised after the location, type and functional form of all the nonlinearities throughout the system are determined. The parameters of the selected model are then estimated using, for instance, linear least-squares fitting. Robust techniques are compared to detect and characterise nonlinearity. The most challenging step, *i.e.* nonlinearity quantification, is achieved utilising the restoring force surface method.

2. THE SMALLSAT SPACECRAFT

The SmallSat structure has been conceived as a low-cost structure for small low-earth orbit satellite [5]. It is a monocoque tube structure which is 1.2 m long and 1 m large. It incorporates 8 flat faces for equipment mounting purposes, creating an octagon shape, as shown in Figure 1 (a). The octagon is manufactured using carbon fibre reinforced plastic by means of a filament winding process. The structure thickness is 4.0 mm with an additional 0.25 mm thick skin of Kevlar applied to both the inside and outside surfaces to provide protection against debris. The interface between the spacecraft and launch vehicle is achieved through 4 aluminium brackets located around cut-outs at the base of the structure. The total mass including the interface brackets is around 64 kg.

The SmallSat structure supports a telescope dummy composed of two stages of base-plates and struts supporting various concentrated masses; its mass is around 140 kg. The telescope dummy plate is connected to the SmallSat top floor via 3 shock attenuators, termed SASSA (Shock Attenuation System for Spacecraft and Adaptator) [6], the behaviour of which is roughly linear and therefore not analysed in the present study. The top floor is a 1 square meter sandwich aluminium panel, with 25 mm core and 1 mm skins. Finally, as depicted in Figure 1 (c), a support bracket connects to one of the 8 walls the so-called Wheel Elastomer Mounting System (WEMS) device which is loaded with an 8 kg inertia wheel dummy. The purpose of this device is to isolate the spacecraft structure from disturbances coming from the inertia wheel through the presence of a soft interface (made up of elastomer plots) between the fixed and mobile parts. In addition, mechanical stops limit the axial and lateral motion of the WEMS mobile part during launch, which gives rise to nonlinear dynamic phenomena. Figure 1 (d) presents a simplified modelling of the WEMS device where the inertia wheel is considered as a point mass. The four nonlinear connections between the WEMS mobile part (the inertia wheel and its cross-shaped support) and fixed part (the bracket and, by extension, the spacecraf itself) are labeled NC 1 – 4 and signaled through black squares. Each nonlinear connection possesses a nonlinear spring (elastomer in traction plus 2 stops) in the axial direction, a second nonlinear spring (elastomer in shear plus 1 stop) in the

(a)

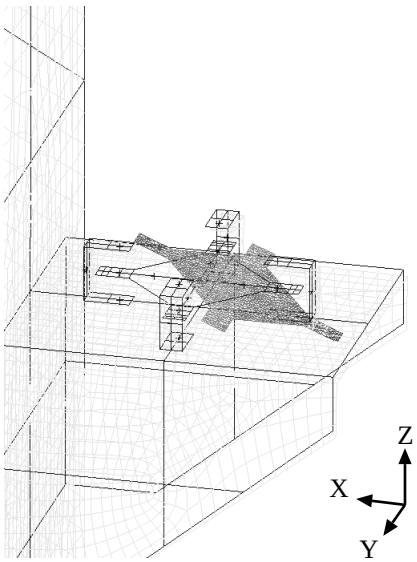

(b)

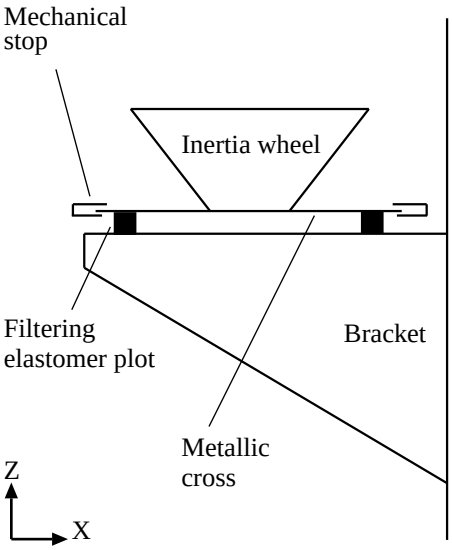

(c)

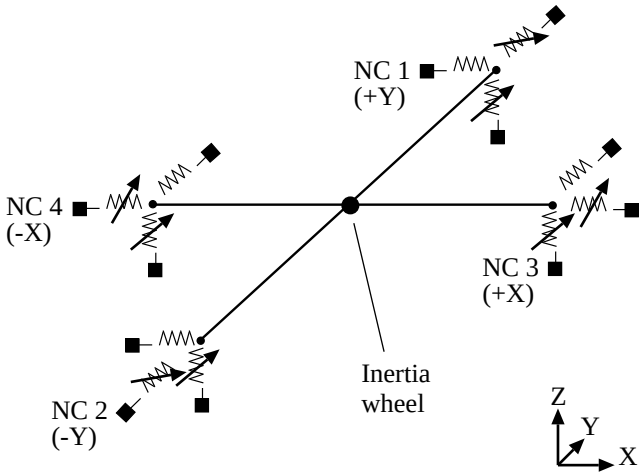

(d)

Figure 1: Picture of the SmallSat and of the WEMS device (a); FEM-based first mode of vibration of the WEMS around 8 Hz — the inertia wheel is considered as a point mass (b); detailed description of the WEMS components (c); simplified modelling of the WEMS mobile part (d).

radial direction and a linear spring (elastomer in shear) in the third direction.

During the experimental test campaign, increasing and decreasing sine-sweep base excitations were applied to the spacecraft for different amplitude levels and directions. This work solely focuses on two data sets measured under 0.6 g and 1 g axial loadings, considering positive sweep rates of 2 and 4 octaves per minute, respectively. In particular, the 1 g excitation corresponded to a qualification test. To further restrict the amount of data analysed in the paper, a single local mode of vibration of the WEMS device will be analysed, located between 7 and 10 Hz. Figure 1 (b) displays its modal shape, involving a concave trajectory along X axis, as predicted by a finite element model (FEM) created in Samcef software.

3. NONLINEARITY DETECTION

Nonlinearity detection basically boils down to seeking departures from linear theory predictions. In that regard, sine-sweep excitations are particularly convenient because, if linear, the structure is known to generate a pure sine wave in output. Nonlinear phenomena are therefore easy to detect by looking for harmonic distortions.

3.1. Visual inspection

Signal distortions in the recorded time series can sometimes be such that a mere visual inspection is sufficient to reveal nonlinear behaviour. Figures 2 (a) and (b) depict the axial relative displacement across the NC 4 measured under 0.6 g and 1 g loadings, respectively. Note that displacement signals were not recorded but were estimated from acceleration measurements through integration using the trapezium rule and high-pass filtering. For confidentiality reasons, displacements were adimensionalised.

At 0.6 g, the resonance peak in Figure 2 (a) shows no visible evidence of nonlinearity. However, a close-up over the 8.2 – 8.5 Hz swept band, as presented in Figure 2 (e), underlines the presence of weak harmonics and small impacts in the oscillations. Impacts occur in negative relative displacement indicating that the mechanical stop is only reached in the -Z direction. At 1 g, a sudden transition at 9.4 Hz from high to low vibration amplitudes is observed in Figure 2 (b) and is an indication of a nonlinear jump phenomenon, proving the activation of a strongly nonlinear regime of motion. Significant harmonics and severe shocks in the -Z direction are also distinguished in the close-up in Figure 2 (f).

3.2. Wavelet transform

The capability of nonlinear systems to generate harmonic components is a powerful detection tool, in particular in the case of sine-sweep excitations. In this context, the wavelet transform (WT) is preferred to the classical Fourier transform because it supports the analysis of signals whose frequency content evolves with time. The wavelet amplitudes of the relative displacements of Figures 2 (a) and (b) are displayed in a logarithmic scale in Figures 2 (c) and (d), respectively. At 0.6 g, impacts occur in a narrow sweep interval around 8.5 Hz and translate into the periodic appearance of a wideband frequency content in the wavelet. At 1 g, mechanical stops are reached over a longer time window, as evidenced in Figure 2 (d). Impacts also appear to be stronger since the wavelet spectrum encompasses higher frequencies. One should remark the expected alignment between the jump phenomenon in Figure 2 (b) and the disappearance of wideband frequency components in Figure 2 (d). Second and third harmonics are also visible in both wavelets but are actually attributed to distortions in the excitation signal. Electrical noise is finally responsible for a frequency line around 50 Hz.

4. NONLINEARITY CHARACTERISATION

Beyond detection, useful insight into the nonlinearity can be gained through visual inspection. For instance, the aforementioned presence of shocks is the symptom of a non-smooth nonlinearity. Moreover, because they only appear for negative relative displacements, the clearance in the -Z direction is found to be smaller than in the +Z direction. This asymmetry can be explained by the prestress induced on the elastomer plots by gravity and was unforeseen during numerical experiments. The amplitude-limiting effect of the stop is also visible within the oscillations in Figure 2 (f) and yields a direct estimation of the -Z clearance around 1.

4.1. Histogram

A particularly meaningful representation of the measured time series for clearance estimation is a histogram. This is achieved in Figures 3 (a) and (b) for the relative displacements of Figures 2 (a) and (b), respectively. The accumulation of samples in the left-hand tail of both distributions confirms the asymmetry of the WEMS device and the location of the clearance around 1. At 1 g, it is worth pointing out that the nonlinear regime is densely populated (it even outnumbers the "linear" distribution) and is covered up to large relative displacements.

4.2. Restoring force surface method

The restoring force surface (RFS) method relies on Newton's second law of motion, written for a single-degree-of-freedom system as

$$m\,\ddot{x} + f(x,\dot{x}) = p \tag{1}$$

where m is the mass, $\ddot{x}$ the acceleration and p the external force and where f encompasses all the restoring forces in the system, being of elastic or dissipative nature. This equation recast into

$$f(x,\dot{x}) = p - m\,\ddot{x} \tag{2}$$

gives a direct access to a non-parametric estimate of the restoring force surface defined by the triplets $(x,\ \dot{x},\ f(x,\dot{x}))$. Applied to more complex systems, the method only provides qualitative information but can still be exploited for visualising nonlinear effects. The NC 4 force-displacement curves at 0.6 g and 1 g are shown in Figures 3 (c) and (d), respectively. They reveal the non-smooth nature of the nonlinearities and the asymmetry in the WEMS behaviour; they also confirm the location of the -Z clearance around 1. In comparison with other techniques, the restoring force curve at 1 g also highlights the activation of the +Z stop, beyond a relative displacement of about 1.5. Damping effects are also visible through the presence of hysteretic loops of dissipation in the two graphs.

5. NONLINEAR PARAMETER ESTIMATION

Nonlinearity quantification is the most challenging step in the identification process but also conveys the most

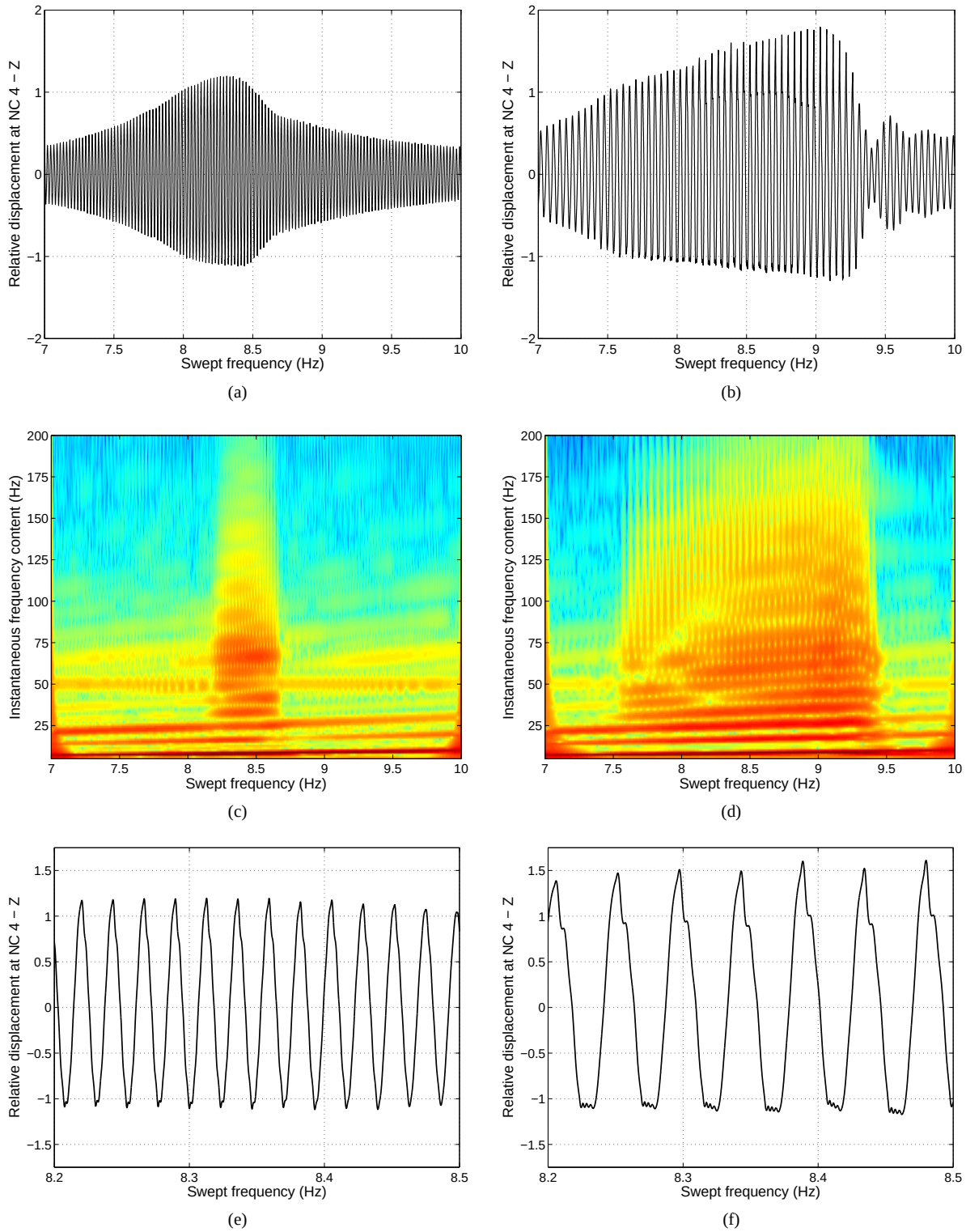

Figure 2: Nonlinearity detection: visual inspection and WT techniques. Left column: measured data at 0.6 g ; right column: measured data at 1 g.

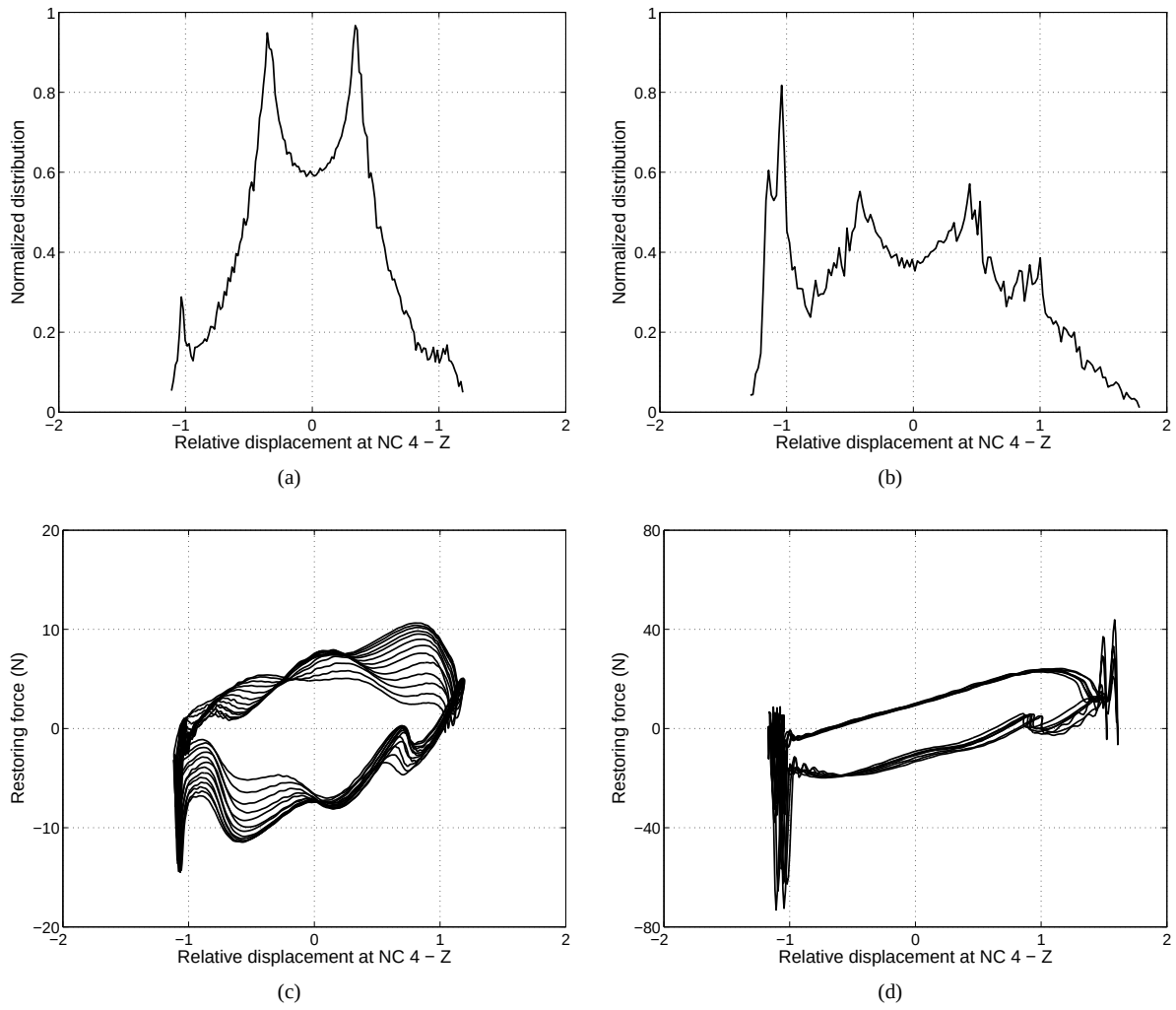

Figure 3: Nonlinearity characterisation: histogram and RFS techniques. Left column: measured data at 0.6 g ; right column: measured data at 1 g.

valuable information. It is even more challenging in the case of a spacecraft because unmeasured sine-sweep excitations are usually considered. In the sequel, a RFS-based method for estimating the WEMS nonlinear stiffnesses is introduced. Numerical investigations of its applicability were conducted in reference [7], where further detail can be found.

5.1. Restoring force surface method

A RFS-based quantification of a multi-degree-of-freedom nonlinear structure is, in general, not possible since it requires a rigorous writing of Newton's law of dynamics. In the case of the WEMS device, however, one can write

$$m\,\frac{\ddot{z}_3+\ddot{z}_4}{2}+f_{NC\,1}+f_{NC\,2}+f_{NC\,3}+f_{NC\,4}=0 \quad (3)$$

where m is the mass of the WEMS mobile part, $\ddot{z}_i$ the axial acceleration measured at the NC i and $f_{NC\,i}$ the associated nonlinear stiffness force. This equation holds for low-velocity time samples only, because it neglects damping forces. Besides, underlying this equation is the assumption that the WEMS mobile part behaves as a rigid body. Rigidity imposes geometrical constraints onto the possible motion of the WEMS. Denoting by $\vec{v}_{12}$ and $\vec{v}_{34}$ the vectors joining opposite NCs, the constraints are

$$\begin{gathered}\tfrac{d\,v_{12}}{dt}=\tfrac{d\,v_{34}}{dt}=0\\ \vec{v}_{12}\cdot\vec{v}_{34}=0\\ \tfrac{\vec{v}_{12}}{2}=\tfrac{\vec{v}_{34}}{2}\end{gathered} \quad (4)$$

and translate, considering the cross-shaped support of the inertia wheel, the invariability of the length of its two arms, their orthogonality and their common midpoints. Figure 4 represents the on-line deviations in $\%$ from these

latter constraints at 1 g level and shows that they are indeed well satisfied. The deformed shape of the vibration mode of interest in Figure 1 (b) explains why the most significant errors occur in X direction.

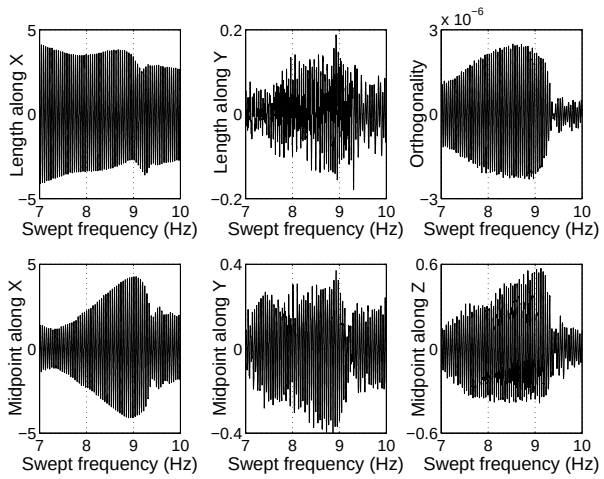

Figure 4: On-line verification of the geometrical conditions of rigidity at 1 g (in $\%$).

In Figure 5, parameter estimation is carried out using Equation (3) but results regarding the NCs 1 and 2 are not displayed because they involve smaller relative displacements. Adimensionalised curve fitting results are provided in the caption of the different graphs. They indicate that the estimations are almost constant regardless of the excitation level, meaning that a reliable identification is achieved. They are also found to be in excellent agreement with the theoretical values implemented in the numerical model, which are 1 and 14.2 for the elastomer and stop stiffnesses, respectively. One should remark that no impact is visible in Figures 5 (a) and (c) whereas the detection analysis proved the activation of nonlinear behaviour at 0.6 g. This is because impacts occur for large velocities that are not considered herein as required by Equation (3). At 1 g, nonlinearity appears even for low-velocity samples and could therefore be accurately assessed.

6. CONCLUSIONS

This paper aimed at identifying a full-scale space structure involving complex nonlinear dynamics from real data. Nonlinearity detection was fairly straightforward through the visual inspection of the measured time series and the WT. Nonlinearity characterisation was then achieved using histograms and the RFS method. They allowed to gain very useful insight into the WEMS nonlinearity, including a reliable estimate of the clearances. Finally, very satisfactory nonlinear parameter estimation was obtained using a RFS-based approach. From this work, it follows that sine-sweep base excitation, which is commonly used in spacecraft testing, is particularly convenient for detecting and characterising nonlinearity. Conversely, because few methods can handle sine-type measurements, random excitation should be preferred for nonlinear parameter estimation. Finally, it is worth stressing that the interface force between the spacecraft and the shaking table is a valuable information that should be recorded for the purpose of nonlinear identification.

ACKNOWLEDGMENTS

This paper has been prepared in the framework of the ESA Technology Research Programme study "Advancement of Mechanical Verification Methods for Nonlinear Spacecraft Structures (NOLISS)" (ESA contract No.21359/08/NL/SFe). Experimental data were measured by EADS-Astrium. The authors also thank Astrium SAS for sharing information about the SmallSat spacecraft.

The authors J.P. Noel and L. Renson would like to acknowledge the Belgian National Fund for Scientific Research (FRIA fellowship) for its financial support.

REFERENCES

[1] S. F. Masri and T. K. Caughey. A nonparametric identification technique for nonlinear dynamic problems. *Journal of Applied Mechanics*, 1979.

[2] C. M. Richards and R. Singh. Identification of multi-degree-of-freedom non-linear systems under random excitations by the reverse-path spectral method. *Journal of Sound and Vibration*, 1998.

[3] V. Lenaerts, G. Kerschen, J. C. Golinval, M. Ruzzene, and E. Giorcelli. Validation of two nonlinear system identification techniques using an experimental testbed. *Shock and Vibration*, 2004.

[4] G. Kerschen, K. Worden, Alexander F. Vakakis, and J. C. Golinval. Past, present and future of nonlinear system identification in structural dynamics. *Mechanical Systems and Signal Processing*, 2006.

[5] A. G. Russell. Thick skin, faceted, CFRP, monocoque tube structure for smallsats. In *European Conference on Spacecraft Structures, Materials and Mechanical Testing*, Noordwijk, The Netherlands, 2000.

[6] P. Camarasa and S. Kiryenko. Shock attenuation system for spacecraft and adaptor (SASSA). In *European Conference on Spacecraft Structures, Materials and Mechanical Testing*, Toulouse, France, 2009.

[7] J. P. Noel, G. Kerschen, and A. Newerla. Application of the restoring force surface method to a real-life spacecraft structure. In *International Modal Analysis Conference*, Jacksonville, FL, 2012.

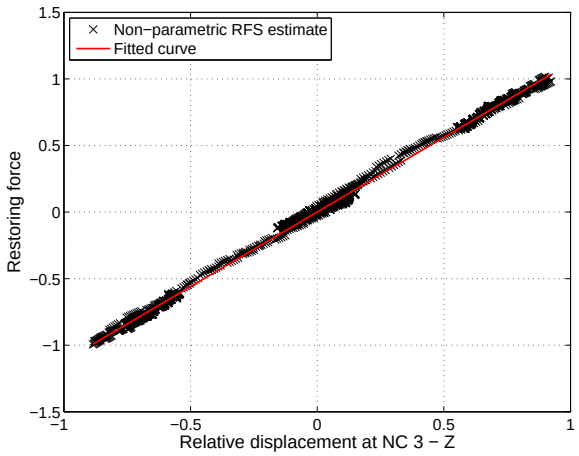

(a) Elastomer stiffness: 1.12.

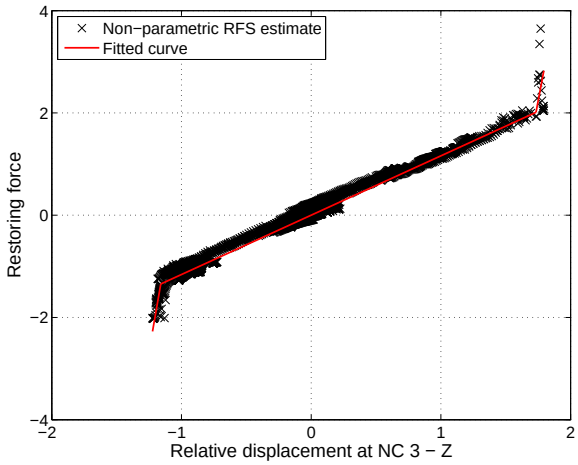

(b) Elastomer stiffness: 1.16; -Z stop stiffness: 13.5; +Z stop stiffness: 12.4.

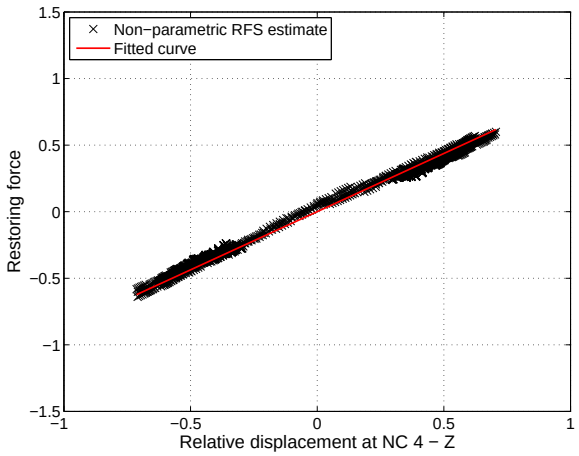

(c) Elastomer stiffness: 0.87.

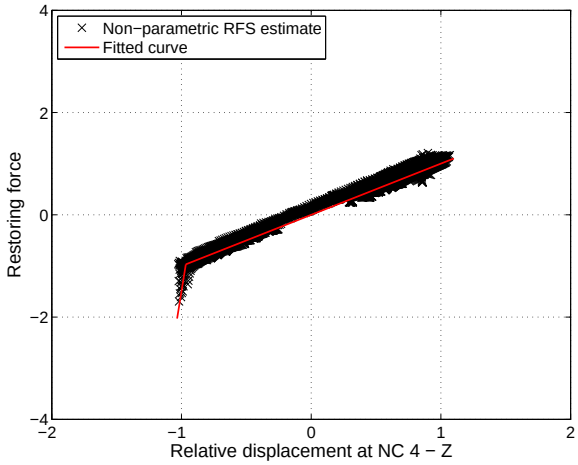

(d) Elastomer stiffness: 1.00; -Z stop stiffness: 14.9.

Figure 5: Nonlinear parameter estimation: RFS technique. Left column: measured data at 0.6 g ; right column: measured data at 1 g.